OXR1 maintains the retromer to delay brain aging under dietary restriction

Pankaj Kapahi (pkapahi@buckinstitute.org)
Buck Institute for Research on Aging https://orcid.org/0000-0002-5629-4947

Kenneth Wilson
Buck Institute for Research on Aging https://orcid.org/0000-0003-3227-9977

Sudipta Bar
Buck Institute for Research on Aging

Eric Dammer
Emory University https://orcid.org/0000-0003-2947-7606

Brian Hodge
Buck Institute for Research on Aging

Enrique Carrera
Buck Institute for Research on Aging

Tyler Hilsabeck
Buck Institute for Research on Aging

Joanna Bons
Buck Institute for Research on Aging

George Brownridge
Buck Institute for Research on Aging

Jennifer Beck
Buck Institute for Research on Aging

Jacob Rose
Buck Institute for Research on Aging

Melia Granath-Panelo
Buck Institute for Research on Aging

Christopher Nelson
Buck Institute for Research on Aging

Alexandra Afenjar
Hôpital Trousseau

Geetanjali Chawla
Regional Centre for Biotechnology https://orcid.org/0000-0003-0354-3716

Rachel Brem
Buck Institute for Research on Aging

Philippe Campeau

University of Montreal https://orcid.org/0000-0001-9713-7107
Hugo Bellen
Howard Hughes Medical Institute https://orcid.org/0000-0001-5992-5989
Birgit Schilling
Buck Institute
Nicholas Seyfried
Emory University https://orcid.org/0000-0002-4507-624X
Lisa Ellerby
Buck Institute for Research on Aging

Biological Sciences - Article

Keywords:

Posted Date: April 7th, 2022

DOI: https://doi.org/10.21203/rs.3.rs-1455343/v1

Additional Declarations: Yes there is potential Competing Interest. Pankaj Kapahi is founder and a member of the scientific advisory board at Juvify Bio.

Version of Record: A version of this preprint was published at Nature Communications on January 11th, 2024. See the published version at https://doi.org/10.1038/s41467-023-44343-3.

Abstract

Dietary restriction (DR) delays aging and neurodegeneration, but the mechanisms behind this remain to be elucidated. We identified genetic polymorphisms in mustard (mtd), the fly homolog of Oxidation resistance 1 (OXR1), which influenced lifespan and mtd expression in neurons in response to DR regulated by the transcription factor Traffic jam (TJ). Knockdown of mtd inhibited DR-mediated lifespan extension. We found that mtd expression naturally declines with age and that loss of mtd destabilized the retromer complex, which regulates trafficking and reuse of endocytosed proteins and lipids and maintains proper lysosomal function. Overexpression of retromer genes Vps35 or Vps26 or pharmacological restabilization with the compound R55 rescued lifespan and neurodegeneration in mtd-deficient flies as well as lysosomal defects in cells from patients who suffer from rapid neurological degeneration caused by loss-of-function of OXR1 variants. Multi-omic analyses in flies and humans showed that decreased Mtd/OXR1 associates with aging and multiple neurological diseases, including Alzheimer's disease, and its overexpression rescued age-related visual decline and tauopathy in a fly model. Hence, OXR1 plays a conserved role in enhancing retromer function and is critical for neuronal health and longevity across species.

main

Aging is a leading contributor to cognitive decline, but dietary restriction (DR) delays aging across species and slows the progression of neurodegenerative diseases[1]; however, the mechanisms that mediate the protective effects of DR in the brain are not fully understood[2]. Additionally, factors such as natural genetic variation greatly influence response to DR, leading to the concept of precision nutrigeroscience to understand how differences between individuals and across tissues modulate responses to diet and influence healthspan and lifespan[2]. We previously used the *Drosophila* Genetic Reference Panel (DGRP)[3] to better understand the genetic effectors of DR-based lifespan response[4], and in this current study, we focus on polymorphisms in the gene *mustard* (*mtd*), which associate with DR-dependent longevity. Genetic variants in the human homolog of *mtd*, *OXR1*, are associated with cerebellar atrophy, hypotonia, language delay, and seizures[5], and its overexpression improves survival in a mouse model of amyotrophic lateral sclerosis (ALS)[6]. Despite the protective properties of OXR1, its biochemical mechanism remains unknown. Here, we identify the dietary and genetic factors which regulate *mtd/ OXR1* and demonstrate its necessity for maintenance of the retromer complex, which is a heteropentameric complex of proteins necessary for recycling transmembrane proteins and lipids from endosomes to the *trans*-Golgi network or the cell membrane[7,8]. We further show that *mtd/ OXR1* regulates a network of genes that are essential for protection against brain aging and neurodegenerative diseases across flies and humans.

Neuronal expression of mtd is required for lifespan extension upon DR

To identify regulators of the protective effects of DR, we measured lifespan under *ad libitum* (AL, 5% yeast) or DR (0.5% yeast) conditions in 160 fly strains from the DGRP[4]. We identified genetic variants in five genes which significantly associated with extreme longevity upon DR (**Extended Data Fig. 1a**). Of these genes, only *Ferredoxin* (*Fdxh*) and *mustard* (*mtd*) have human orthologs (*ferredoxin 2* and *oxidation resistance 1*, *OXR1*, respectively). We found that an allele in *mtd* consisting of a single-nucleotide polymorphism, a deletion of 129 base pairs, and an insertion of 101 base pairs associated with reduced lifespan under DR, but not AL, when compared to the wild-type allele (**Fig. 1a**). Whole-body mtd^{RNAi} driven by *Act5c*-GS-*Gal4* (**Fig. 1b**), but not $Fdxh^{RNAi}$ (**Extended Data Fig. 1b**), resulted in DR-specific reduction in lifespan. In contrast, a strong null allele *mtd-T2A-Gal4* strain ($mtd^{MI02920\text{-}T2A\text{-}Gal4}$)[5] caused lethality in development and DR did not extend lifespan in the flies that survived to adulthood (**Fig. 1c**). *OXR1* loss in humans is associated with severe neurological defects and premature death[5] whereas overexpression provides protection in a mouse model of amyotrophic lateral sclerosis[6], yet its cellular mechanism of action is unknown. *OXR1* is often studied for its role in oxidative stress response[9,10], but Wang *et al.* showed that its loss causes lysosomal dysfunction independent of oxidative stress [5]. Thus, identifying the mechanism of OXR1 will elucidate a valuable target for neuroprotection.

DR induced a seven-fold increase in *mtd* mRNA expression in the head but a 52% reduction in the abdomen (**Fig. 1d**). Neuronal mtd^{RNAi} driven by the constitutively active *elav-Gal4* induced developmental defects and severe lifespan reduction under both diets (**Fig. 1e**), similar to loss of *mtd*. These phenotypes were not observed with intestine- or glia-specific mtd^{RNAi} (**Extended Data Fig. 1c-d**). To evaluate the impact of neuronal mtd^{RNAi} with age, we used the conditional RU486-inducible *elav*-GS-*Gal4* driver to induce a milder knockdown only in adulthood. This eliminated DR-mediated lifespan extension but did not alter lifespan on AL (**Fig. 1f and Extended Data Fig. 1e**). The TLDc domain in Mtd/OXR1 is responsible for neuroprotection[5,11], so we overexpressed truncated human *OXR1* containing this domain ($hOXR1^{OE}$) in neurons of flies which harbored the *mtd* null allele and observed a complete rescue of lifespan and DR response (**Fig. 1g**). Neuronal $hOXR1^{OE}$ in a wild-type background extended lifespan only under DR (**Fig. 1h**). *mtd* expression was significantly increased across life in wild-type flies under DR, but this expression declined from day 7 to day 21 on both diets (**Extended Data Fig. 1f**). Overall, these results demonstrate that neuronal *mtd* expression is elevated by DR, declines with age, and is necessary and sufficient for DR-mediated lifespan extension.

Traffic jam promotes *mtd* expression diet- and allele-specifically

In the DGRP, strains with the long-lived allele had elevated *mtd* expression in the head under DR, unlike strains that harbor the short-lived allele (**Fig. 1i**). Strains with the long-lived allele showed elevated expression of *mtd* transcripts that include exons 3' of the variant only (**Extended Data Fig. 1g**). However, transcripts with exons from both sides of the variant (“long transcripts”) showed elevated expression on DR regardless of allele (**Extended Data Fig. 1h**). To validate the effects of these alleles, we cloned the allelic region into luciferase reporter constructs and transfected S2 cells. Upon serum withdrawal to mimic DR, luciferase activity was elevated only in cells with the long-lived sequence (**Fig. 1j**), suggesting

that it influences nutrient-dependent changes in *mtd* expression. Using publicly available fly ChIP-seq data[12,13], we found significant binding signal at this locus for CCCTC-binding factor (CTCF) and Traffic jam (TJ) (**Extended Data Fig. 1i**). Inducible neuronal *ctcf*^{RNAi} increased *mtd* expression (**Extended Data Fig. 1j**), whereas *tj*^{RNAi} reduced expression of all *mtd* transcripts under DR (**Fig. 1k**) and shortened lifespan specifically under DR (**Fig. 1l**). We validated that TJ, the fly homolog of MAF, binds this locus via ChIP-PCR (**Extended Data Fig. 1k**). In summary, we found that natural variants in mtd that show increased expression upon DR are regulated by Traffic Jam and are associated with lifespan extension upon DR.

mtd regulates the retromer complex

To define the pathway affected by loss and gain of Mtd/OXR1, we analyzed gene ontology (GO) terms for the top 50 genes that show co-expression patterns similar to human OXR1 (**Supplementary Data 2**)[14]. These showed significant enrichment for protein trafficking from the endosome to the lysosome or recycling endosomes (**Fig. 2a and Supplementary Data 3**). Neuronal *mtd*^{RNAi} increased levels of Atg8a-II (fly ortholog of LC3), a marker for autophagosome formation (**Fig. 2b**), consistent with the lysosomal accumulation phenotype observed in human fibroblasts and flies with *OXR1* deficiency[5]. We co-stained human fibroblasts[5] for OXR1 and markers for vesicular transport organelles (lysosome, endosome, Golgi, endoplasmic reticulum, and mitochondria). OXR1 staining overlapped most with the endosomal marker RAB7 (**Extended Data Fig. 2a**). As retromer dysfunction at the endosome causes lysosome dysfunction[15] as well as increased autophagosome formation[16] due to improper trafficking of endocytosed proteins and lipids, we hypothesized that OXR1 maintains retromer function. Neuronal *mtd*^{RNAi} and *tj*^{RNAi} significantly reduced the levels of retromer proteins (**Fig. 2c-d**). This was not due to reduced retromer gene transcription under *mtd*^{RNAi} (**Extended Data Fig. 2b**). Co-staining fly brains with antibodies against Mtd and retromer protein Vps35 with neuronal *mtd*^{RNAi} also showed that Vps35 was reduced with *mtd*^{RNAi} (**Fig. 2e**). We also also observed co-localization of Vps35 and Mtd in the brains of *w*^{1118} control flies (**Fig. 2f**). Retromer maintenance is necessary for neuronal health[17,18], and the loss of retromer proteins like VPS35 induces neurodegenerative disease progression[19,20]. Our results indicate that Mtd is involved in the maintenance of retromer function.

Retromer stabilization rescues Mtd/OXR1 deficiency

Next, we tested if enhancing retromer function rescues *mtd*^{RNAi} phenotypes. Neuronal overexpression (by *elav-Gal4* driver) of *vps35* or *vps26* rescued fly larval lethality (**Fig. 3a**) and lifespan (**Fig. 3b**). Overexpression of *vps35* also recovered the loss of lifespan extension by DR in *mtd*^{RNAi}. Moreover, pharmacological retromer stabilization with the compound R55[21] also rescued developmental deformities (**Fig. 3c**) and the shortened lifespan of flies with *mtd*^{RNAi} (**Fig. 3d**). R55 further extended lifespan under DR beyond that of control strains on DR (**Fig. 3d-e**). However, simultaneous *mtd*^{RNAi} and overexpression of autophagy genes *Atg8*, *Atg6*, or *LAMP1* did not rescue developmental defects

(**Extended Data Fig. 3a**), suggesting that defects due to *OXR1* deficiency are not due to a reduction in autophagic function.

Retromer stabilization by R55 rescued VPS35 levels and VPS35 co-localization with OXR1 in human fibroblasts from patients with *OXR1* mutations[5] (**Fig. 3f**). This *OXR1* mutation did not change RAB7 levels, indicating that endosome formation was unaltered (**Extended Data Dig. 3b**). R55 also significantly reduced the number of lysosomes in the *OXR1*-deficient cells (**Fig. 3g**). Lysosomal protease Cathepsin B was significantly increased in OXR1 disease fibroblasts and further increased with R55 (**Fig. 3h**), despite the decreased lysosomal number in R55-treated cells. To further examine lysosomal activity, we compared LC3B-II levels in fibroblasts treated with the V-ATPase inhibitor bafilomycin, which blocks autophagy to demonstrate accumulated autophagosome pool size, to LC3B-II levels without bafilomycin, which represent steady state pool size as LC3B-II is turned over during autolysosome formation[22]. *OXR1*-deficient fibroblasts had significantly reduced basal LC3B-II compared to control cells, whereas blocking LC3B turnover with bafilomycin showed significantly greater LC3B-II levels than control cells, indicating increased LC3B turnover in the *OXR1*-deficient cells. Treatment with 10 μM R55 increased the basal levels of LC3B-II in *OXR1*-deficient fibroblasts, rescuing the LC3B-II levels compared to the deficient cells not treated with R55 (**Fig. 3i**, additional statistics in **Supplementary Data 1**). These results suggest that retromer stabilization rescues altered autophagic activity in human cells with *OXR1* mutations and lifespan defects caused by *mtd* -deficiency in flies.

Retromer stabilization rescues sensory decline induced by *mtd*^{RNAi}

To determine how *mtd/OXR1* deficiency influences brain aging, we analyzed the transcriptomes of heads from younger (day 7) and older (day 21) flies with and without neuronal *elav*-GS-*Gal4*-induced *mtd*^{RNAi} through principal component analysis (PCA). Younger *mtd*^{RNAi} DR transcriptomes grouped with younger AL flies and older DR flies, whereas transcriptomes from older *mtd*^{RNAi} DR flies grouped with older AL flies, suggesting that *mtd*^{RNAi} accelerated transcriptional signatures towards older flies (**Fig. 4a and Supplementary Data 4**). GO term analysis for *mtd*^{RNAi} showed significant downregulation of genes associated with rhabdomere development and stimulus detection (**Fig. 4b and Supplmentary Data 5**), which have been implicated in retromer dysfunction in flies[19,23]. We observed delayed age-related visual decline upon DR, but this protective effect was abrogated by neuronal *mtd*^{RNAi} (**Fig. 4c**). The ommatidia of the RNAi flies were significantly more disordered than in controls (**Fig. 4d**). We assessed negative geotaxis but observed no change in activity between flies with or without neuronal *mtd*^{RNAi}, though activity was enhanced by DR (**Fig. 4e**), suggesting an uncoupling of activity and eye degeneration. To determine if accelerated sensory decline was restricted to the visual system, we tested chemotaxis throughout lifespan. Neuronal *mtd*^{RNAi} under DR conditions induced more rapid decline in response to the attractant than DR controls whereas flies under AL conditions were unaffected by RNAi (**Fig. 4f**), suggesting impaired signaling for two phenotypes commonly disrupted in age-related neurodegenerative diseases, vision and olfaction[24,25]. Pan-neuronal *hOXR1*^{OE} improved phototaxis throughout life under DR (**Fig. 4g**). Retromer stabilization by *vps26*^{OE} or *vps35*^{OE} rescued phototaxis response in *mtd*^{RNAi} flies, as

did treatment with 6 μM R55 (**Fig. 4h-i**). We observed no significant changes in body mass, triglyceride levels, or starvation resistance upon inducible pan-neuronal induction of *mtd*^{RNAi} (**Extended Data Fig. 4a-c**). These results indicate that *mtd* and the retromer are necessary for age-associated maintenance of the fly neuronal sensory systems but not changes in triglyceride metabolism.

mtd/ OXR1 expression protects against neurodegenerative diseases and Alzheimer's phenotypes

To identify disorders associated with *mtd/ OXR1*, we determined proteins significantly downregulated in flies with neuronal *mtd*^{RNAi} via data-independent acquisition mass spectrometry (q value < 0.05, **Supplementary Data 6-7**)[26]. This revealed significant enrichment for proteins involved in multiple human neurodegenerative diseases (**Extended Data Fig. 4d**). We next analyzed -omics datasets from humans to learn more about the conserved nature of OXR1 in neurodegenerative diseases. We found an overlap of 83 genes between proteins with abundance levels that positively correlate with OXR1 (ρ > 0.30, **Supplementary Data 8**) from the Accelerating Medicines Partnership – Alzheimer's Disease (AMP-AD) dataset[27] and genes affected by age from the Genotype-Tissue Expression (GTEx) project (**Fig. 4j and Supplementary Data 9**)[28,29]. KEGG pathway analysis for the genes which overlapped between these datasets revealed significant enrichment for age-related neurodegenerative diseases including Alzheimer's, Huntington's, and Parkinson's diseases, (**Fig. 4k and Supplementary Data 10**)[30]. Retromer dysfunction has been associated with age-related neurodegenerative diseases that are protected by DR, including AD[31-34], especially in trafficking cargo involved in disease progression[21]. We therefore also analyzed human OXR1 and retromer-associated protein abundance using the AMP-AD dataset[35]. Lower levels of OXR1, VPS35, SNX5, and RAB7A were all significantly associated with AD diagnosis and poor memory and pathology scores (**Fig. 4l and Extended Data Fig. 4e**). To determine if OXR1 or retromer overexpression could rescue phenotypes associated with AD and tau pathogenesis, we neuronally overexpressed *hOXR1*, *vps35*, or *vps29* in flies with simultaneous *GMR*-driven pathogenic human *Tau* in the eyes. Flies with *hTau*^{OE} alone showed rapid eye degeneration, but neuronal *hOXR1*^{OE}, *vps35*^{OE}, or *vps29*^{OE} rescued this phenotype (**Fig. 4m**). These results demonstrate that the proteins in OXR1's network play a critical and conserved role in humans and flies for brain aging and neurodegeneration.

Discussion

The widespread health and longevity benefits of DR are well-established, but the mechanisms by which DR mediates brain-specific functions are poorly understood. We previously showed in flies that DR elicits protective effects on lifespan and healthspan at least partially through distinct mechanisms[4]. While nutrient signaling pathways, such as TOR and ILS, are potential anti-aging pathways with roles in enhancing metabolism and burning fat[36], the variability in response to DR across different individuals and in different tissues suggests there are still many molecular mechanisms that remain unelucidated[37]. While screening for DR-responsive mechanisms, we found a role for *mtd/ OXR1* in regulating neuronal health with age and in response to DR. Here, we showed that *mtd/ OXR1* is an essential gene for healthy brain aging. We found that alleles of *mtd* that are upregulated by DR are regulated by the transcription

factor TJ, and that this expression is necessary DR-mediated lifespan extension. Mtd/OXR1 maintains the retromer complex, and retromer stabilization rescues lysosomal and longevity defects induced by *mtd/ OXR1* deficiency. Our work presents a novel mechanism by which DR slows brain aging through the action of OXR1 and its downstream effect on the retromer.

Retromer function is necessary for neuron survival[17,38,39]. Thus, elucidating novel retromer pathway components is valuable for promoting brain health, especially with aging. Retromer dysfunction has been associated with age-related neurodegenerative diseases that are protected by DR, including Alzheimer's[31,40-42], Parkinson's[19,43-45], and Huntington's diseases[46], especially in trafficking cargo involved in disease progression, such as APP [21] and β-secretase[47]. Mtd/OXR1 provides a linchpin for this interactive relationship between retromer regulation and DR-mediated neuroprotection with age. Our findings with OXR1's regulation of retromer function resemble those of PLA2G6, which interacts directly with VPS26 and VPS35[19]. PLA2G6 maintains the retromer to improve ceramide trafficking[19]. Importantly, our work also shows that the effects of OXR1 on the retromer complex influence the lysosomal phenotypes in patients with *OXR1* deficiencies, as this phenotype was rescued in patient cells supplemented with R55. These findings suggest that *OXR1* is a necessary component to gain the benefits of autophagy, especially under DR conditions, and that these benefits are mediated by OXR1's regulation of retromer function.

We further demonstrate that the *OXR1* gene network, conserved in flies and humans, is an important target for brain aging and neurodegenerative diseases. Loss of *mtd* accelerated aging and visual decline in flies, but this was rescued by retromer stabilization. Additionally, overexpression of *OXR1* rescued age-related visual decline as well as transgenically-induced tauopathy in a fly model. Our work implicates OXR1 and its network as a key regulators and potential therapeutic targets to slow aging and age-related neurodegenerative diseases across flies and humans.

Methods

Genome-wide association analysis

We used DGRP release 2 genotypes, and FlyBase R5 coordinates for gene models. We used only homozygous positions and a minor allele frequency of ≥25% to ensure that the minor allele was represented by many observations at a given polymorphic locus[48]. We grouped the DGRP lines reared on a diet into a top 25 in-case group and a non-case group (>41 days median lifespan in DR conditions). The genotype distributions at each locus in these groups were compared via Fisher's exact test using the SciPy.stats module in Python[49]. The genotypes were arranged in the contingency table configuration [[#CaseRefAllele/#CaseAltAllele], [#NonCaseRefAllele/#NonCaseAltAllele]]. Nominal p-values denoted as "P value" in **Extended Data Fig. S1a** report the probability that the relative proportions of one variable are independent of the second variable. To avoid the potential for false positives at a given nominal cutoff owing to p-value inflation, we calculated false discovery rates via permutation as follows: for a given permutation i, we randomized phenotype values across DGRP lines, and assigned in- vs non-case

designations on this permuted data set before we carried out Fisher's exact tests for each marker in turn as above. We counted the number of markers n^i that scored above a given p-value threshold t. We tabulated the false discovery rate at t as the ratio between the average n^i across 10 permutations and the number of markers called at t in the real data.

Gene expression and proteomic analyses

To determine gene expression in a normal system, we sampled 50 heads from mated females *of* w^{1118} control strain after 1 week on an AL or DR diet. We isolated RNA using Zymo Quick RNA MiniPrepkit (R1054) (Zymo Research, Irvine, CA). For qRT-PCR, we used Superscript III Platinum SYBR Green One-Step qRT-PCR kit from Invitrogen, Carlsbad, CA (11736-051) and followed the manufacturer's instructions with a Roche Lightcycler 480 II machine. Primer used are listed at the end of the Methods. To validate the effects of RNAi or mutation on gene expression, we collected 5 whole flies, 10 thoraces, 5 abdomens, or 50 heads after 1 week on AL or DR, depending on the body part being analyzed. We then isolated RNA from these samples and performed qRT-PCR on the perturbed genes as described. RNA sequencing was performed by UC Berkeley QB3 Functional Genomics Laboratory, and reads were analyzed with the use of Bowtie2 read alignment package[50,51].

Fly strains used in this study

All flies were obtained from Bloomington Stock Center[52], Vienna *Drosophila* Resource Center[53], or FlyORF[54] and outcrossed six times to our lab control strains. Each line was mated and developed on a standard laboratory diet (1.5% yeast). At 2–3 days post-eclosion, mated female progeny were transferred to AL (5.0% yeast extract) or DR (0.5% yeast extract) diet via CO_2, as described[55]. Living flies were transferred to fresh vials every other day and dead flies were recorded until all flies were deceased. Flies were maintained in a 12-h light/dark cycle in a room maintained at 25^{o}C and 65% relative humidity[56]. A detailed list of fly strains used can be found at the end of the Methods section.

Fly phenotyping

We used the whole-body GeneSwitch driver *Act5C*-GS-*Gal4*, neuron-specific inducible driver *elav*-GS-*Gal4*, constitutively active *elav-Gal4* driver, glia specific *repo-Gal4*, or eye-specific *rdgA-Gal4* for directed RNAi. 15 virgin driver females were mated with three transgene line males in four bottles containing a standard diet. At 2–3 days after progeny eclosion, mated females were sorted onto AL or DR media with or without 200 μM RU486 (final concentration) for inducible RNAi activation[56,57], and flies were maintained on these media for life. Body mass was measured in five replicates of three flies using a Radwag 82/220.X2 analytical balance. Flies were then frozen, and triglycerides were measured using Stanbio Triglycerides LiquiColor Test. Glucose was measured using Stanbio Liqui-UV Hexokinase kit. For both assays, absorbance was measured using SpectroMax M2 spectrophotometer. Starvation was performed as described[56] by rearing adult flies for 10 days on an AL diet and then transferring to medium containing water and 1% agarose. Flies were checked for deaths every 4 h until all flies were deceased. Pupariation

rate was determined by mating flies and placing 60 resulting embryos on an AL diet. Number of pupae formed was recorded daily. For western blot analysis, fly heads were homogenized in TPER lysis buffer and protein concentrations were determined by BCA. Western blots were quantified using ImageQuant. List of antibodies is provided at the end of Methods section. Negative geotaxis was performed by placing flies in empty vial and counting proportion of flies that climbed 6 cm within 10 sec. Three replicates were performed per vial, as described[4]. Phototaxis was performed by placing flies in on end of a 30-cm horizontal tube and shining light at one end. The proportion of flies that had travelled to the last 10 cm at the other end was recorded. Chemotaxis was performed by placing flies in a tube with one end containing a cotton plug saturated with 1 mL of 1-hexanol attractant, the other end with water. The proportion of flies in the segment with 1-hexanol after 30 sec was recorded[58]. Starvation, lifespan, phototaxis, chemotaxis, and geotaxis assays were performed with approximately 200 starting adult flies, except for constitutively active *mtd*^{RNAi} and *mtd* mutant flies, since few flies reach development in these strains. Rough eye phenotype was analyzed using Flynotyper plug-in in Image J[59]. Images were taken with Olympus BX51 with 10X objective using fiber optics gooseneck microscope illuminator. 10-12 optical slices were taken and reconstitute using Zerenestacker (Zerene Systems, Richland, WA).

Cell lines used in this study

Drosophila S2 cells were cultured in Schneider's medium supplemented with 10% heat-inactivated FBS and penicillin-streptomycin at 25°C. For inducing starvation for luciferase reporter analysis, cells were washed in PBS and re-suspended in PBS supplemented with 20 mg/ml glucose for 12 h. Patient cell lines were generated from skin biopsies and were maintained as described in DMEM supplemented with 15% fetal bovine serum and 1% antibiotic cocktail[5]. Cells were maintained at 37^{o}C. Cells undergoing serum withdrawal were treated with medium without fetal bovine serum. The OXR1 deletion line is from a female patient. Cell lines and media are described at the end of the Methods.

Transient transfections

Transfections of S2 cells with the luciferase reporter plasmids were performed using Lipofectamine 3000 (Thermo Fisher Scientific). For 1.5 X 10^6 cells, 450 ng of S-188-cc-Rluc and 450 ng of the enhancer driven S-188-cc-Luc were used. For each transfection, 10 ml of P3000 and 4 ml of Lipofectamine 3000 reagent were used. Starvation was induced 48 h after the transfection, and cells were harvested for reporter assay 58–60 h after the transfection. All enhancer S-188-cc-Luc constructs were generated by PCR cloning. PCR was performed with the Phusion High-Fidelity DNA polymerase (Thermo Fisher Scientific). All reporter constructs were verified by sequencing. The primers used for cloning and sequencing are listed below.

Luciferase reporter assays

The reporter plasmids were designed for use with the Dual-Luciferase reporter system (Promega Corp., Madison,WI), with firefly luciferase as the primary reporter and Renilla luciferase as an internal transfection control[60]. Cells were extracted and reporter activities measured with the Dual-Luciferase

Assay kit (Promega Corp.), according to a slightly modified version of the manufacturer's protocol. Unless otherwise stated, data represent the mean of at least three independent experiments, with error bars indicating SD.

Fibroblast lysates

Treatments with 10 μM R55 (Sigma-Aldrich #531084) were conducted for 48 h. Bafilomycin (100 nM, Cayman Chemical #11038) or DMSO control (Sigma Aldrich #276855) treatment was for 4 h prior to lysate collection. Lysates were collected with MPER lysis buffer and sonicated. Protein concentrations were determined by BCA. Western blots were quantified using ImageQuantTL.

LysoTracker

Fibroblasts were plated in 8-well chamber slides and maintained for 48 h before supplementation with R55 or DMSO control for another 48 h. LysoTracker Deep Red (Thermo Fisher Cat#L12492) was diluted 1:2000 in medium for lysosome staining and Hoechst 33342 solution (Thermo Fisher Cat#62249) was diluted 1:1000 in medium for nuclear staining. Cells were incubated with stains for 30 min at 37^{o}C and then washed with medium and immediate imaged and analyzed using BioTek Cytation 5 Imaging Reader. Mean intensity of red fluorescence per nucleus was quantified.

Immunocytochemistry

After the treatments described above, cells were fixed in 4% paraformaldehyde in PBS. After three washes with PBS, cells were permeabilized using 0.1% Triton X-100 solution and blocked for 1 at room temperature with 1% bovine serum albumin and 5% donkey serum in PBS. Primary antibodies were diluted in blocking buffer and cells were incubated overnight at 4^{o}C. After three washes with PBS, secondary antibodies (1:1000) were added and incubated for 1.5 h at room temperature. Slides were mounted with ProLong Gold antifade reagent with DAPI (Invitrogen Cat#P36931). Cells were imaged and analyzed using BioTek Cytation 5 Imaging Reader. List of antibodies used is provided at the end of Methods section.

Immunohistochemistry

Adult *Drosophila* brains were dissected in PBS and immediately fixed in 4% PFA for 30 min. Post-fixation washes were done in PBS, and permeabilization was done in PT (PBS with 0.3% Triton X-100), three times for 30 min each. Blocking of tissues was done in permeabilization solution with 0.5% BSA. The brains tissue was labeled with primary antibodies (1:100) overnight in 4^{o}C, followed by three washes with PT solution. Secondary antibody incubation was for 2 h at room temperature. Tissues were then washed three times with PT and mounted with Fluoromount G mounting medium. All incubation steps were done with continuous mild shaking. Images were taken in Zeiss LSM 780 confocal microscope. List of antibodies used is provided at the end of Methods section.

Proteomic analysis

Analyses were performed in house as described in Supplementary data. Briefly, heads from adult flies with or without pan-neuronal *mtd*^{RNAi} were collected and flash frozen in liquid nitrogen in 5 replicates of at least 20 heads on the day of eclosion per replicate pool. Frozen heads from each condition/replicate were immersed in 100 µL of lysis buffer containing 4% SDS, 8 M urea, 200 mM triethylammonium bicarbonate (TEAB) at pH 8, 75 mM sodium chloride, 1 µM trichostatin A, 3 mM nicotinamide, and 1x protease/phosphatase inhibitor cocktail (Thermo Fisher Scientific, Waltham, MA). Lysates were subsequently homogenized for 2 cycles with a Bead Beater TissueLyser II (Qiagen, Germantown, MD) at 24 Hz for 3 min each, and further sonicated. Lysates were clarified by spinning at 15,700 x *g* for 15 min at 4°C, and the supernatants containing the soluble proteins were collected. Protein concentrations were determined using a Bicinchoninic Acid Protein (BCA) Assay (Thermo Fisher Scientific, Waltham, MA), and subsequently 100 µg of protein from each sample were aliquoted. Samples were then solubilized using 4% SDS, 50 mM TEAB at a pH 8. Proteins were reduced using 20 mM DTT in 50 mM TEAB for 10 min at 50°C followed by 10 min at RT, and proteins were subsequently alkylated using 40 mM iodoacetamide in 50 mM TEAB for 30 min at room temperature in the dark. Samples were acidified with 12% phosphoric acid to obtain a final concentration of 1.2% phosphoric acid, and diluted with seven volumes of S-Trap buffer (90% methanol in 100 mM TEAB, pH ~7). Samples were then loaded onto the S-Trap mini spin columns (Protifi, Farmingdale, NY), and spun at 4,000 x *g* for 10 seconds. The S-Trap columns were washed with S-Trap buffer twice at 4,000 x *g* for 10 seconds each. A solution of sequencing grade trypsin (Promega, San Luis Obispo, CA) in 50 mM TEAB at a 1:25 (w/w) enzyme:protein ratio was then added, and after a 1-hour incubation at 47°C, trypsin solution was added again at the same ratio, and proteins were digested overnight at 37°C. Peptides were sequentially eluted with 50 mM TEAB (spinning for 1 min at 1,000 x *g*), 0.5% formic acid (FA) in water (spinning for 1 min at 1,000 x *g*), and 50% acetonitrile (ACN) in 0.5% FA (spinning for 1 min at 4,000 x *g*). After vacuum drying, samples were resuspended in 0.2% FA in water, desalted with Oasis 10-mg Sorbent Cartridges (Waters, Milford, MA). All samples were vacuum dried and resuspended in 0.2% FA in water at a final concentration of 1 µg/µL. Finally, indexed retention time standard peptides, iRT (Biognosys, Schlieren, Switzerland)[61] were spiked into the samples according to manufacturer's instructions. The solvent system consisted of 2% ACN, 0.1% FA in water (solvent A) and 98% ACN, 0.1% FA in water (solvent B). Briefly, proteolytic peptides (2 µg) were loaded onto an Acclaim PepMap 100 C18 trap column with a size of 0.1 x 20 mm and 5 µm particle size (Thermo Fisher Scientific) for 5 min at 5 µL/min with 100% solvent A. Peptides were eluted on to an Acclaim PepMap 100 C18 analytical column sized as follows: 75 µm x 50 cm, 3 µm particle size (Thermo Fisher Scientific) at 0.3 µL/min using the following gradient of solvent B: 2% for 5 min, linear from 2% to 20% in 125 min, linear from 20% to 32% in 40 min, and up to 80% in 1 min, with a total gradient length of 210 min. Samples were analyzed by nanoLC-MS/MS in data-independent acquisition (DIA) mode[62,63] using a variable window isolation scheme[26] on the Orbitrap Eclipse Tribrid platform (Thermo Fisher Scientific, San Jose, CA). Samples were acquired in data-independent acquisition (DIA) mode. Full MS spectra were collected at 120,000 resolution (AGC target: 3e6 ions, maximum injection time: 60 ms, 350-1,650 m/z), and MS2 spectra at 30,000 resolution (AGC target: 3e6 ions, maximum injection time: Auto, NCE: 27, fixed first mass 200 m/z). The DIA precursor ion isolation scheme consisted of 26 variable windows covering

the 350-1,650 m/z mass range with an overlap of 1 m/z[26]. DIA data was processed in Spectronaut v15 (version 15.1.210713.50606; Biognosys) using directDIA. Data was searched against the *Drosophila melanogaster* proteome with 42,789 protein entries (UniProtKB-TrEMBL), accessed on 12/07/2021. Trypsin/P was set as digestion enzyme and two missed cleavages were allowed. Cysteine carbamidomethylation was set as fixed modification, and methionine oxidation and protein N-terminus acetylation as variable modifications. Data extraction parameters were set as dynamic. Identification was performed using 1% precursor and protein q-value (experiment). Quantification was based on MS2 area, and local normalization was applied; iRT profiling was selected. Differential protein expression analysis was performed using a paired t-test, and p-values were corrected for multiple testing, specifically applying group wise testing corrections using the Storey method[64]. Protein groups with at least two unique peptides, q-value < 0.05, and absolute Log2(fold-change) > 0.58 were considered to be significantly changed comparing *mtd*^{RNAi} to TRiP control strain, and are listed in Supplementary data.

Gene ontology analyses

GO term analysis of *Drosophila* genes was performed using the set of all genes downregulated on day 14 from our RNA sequencing dataset. Analysis was performed using Gene Ontology enRIchment anaLysis and visuaLizAtion tool (GOrilla) and Process, Function, and Component analyses were all represented. For genes co-expressed with human OXR1, the top 50 genes from ARCHS[4] tool[14] were analyzed using ENRICHR GO Cellular Component 2021 Ontology list[30].

Quantification and statistical analysis

Significance of differences between survival curves was assessed by log rank test. $p<0.05$ was considered statistically significant. Error bars represent SD across at least three biological replicates. Significant differences between experimental groups and controls are indicated by *. *, $p < 0.05$, **, $p < 0.005$, ***, $p < 0.0005$, determined by unpaired t test. nc = no change, ns = not significant. Statistical analyses were calculated with GraphPad Prism 4. Additional statistical details, including starting n for each experiment, can be found in Supplementary Data 1. Quantification of cell images was performed using BioTek imaging software. Statistics for genome-wide analyses were performed as previously stated.

Drosophila melanogaster strains used		
Strain	**Source**	**ID number**
Drosophila Genetic Reference Panel strains	Bloomington Drosophila Stock Center	All DGRP strains
Act5C-GS-Gal4 Driver (inducible, whole body) P{w[+mC]=Act5C(FRT.y[+])GAL4.Switch.PR}X, y[1] w[*]	Bloomington Drosophila Stock Center	#9431
Elav-GS-Gal4 Driver (inducible, neuronal) w1118 ; P{w[+mC]=elav-Switch.O}GSG301	Bloomington Drosophila Stock Center	#43642
Elav-Gal4 Driver (non-inducible, neuronal) P{w[+mW.hs]=GawB}elav[C155]	Bloomington Drosophila Stock Center	#458
5966-GS-Gal4 (inducible, intestinal) +; 5966-GS	Provided by lab of Dr. David Walker, University of California, Los Angeles	N/A
repo-Gal4 (non-inducible, glial) w[1118]; P{w[+m*]=GAL4}repo/TM3, Sb[1]	Bloomington Drosophila Stock Center	#7415
GMR-driven mutant Tau (non-inducible, eye), Elav-Gal4 (non-inducible, neuronal) P{w[+mW.hs]=GawB}elav[C155]; P{w[+mC]=GMR-htau/Ex}1.1	Bloomington Drosophila Stock Center	#51360
w^{1118} control strain	Bloomington Drosophila Stock Center	#5905
Transgenic RNAi Project (TRiP) control strain y[1] sc[*] v[1]; P{y[+t7.7] v[+t1.8]=VALIUM20-mCherry}attP2	Bloomington Drosophila Stock Center	#35785
mtd RNAi y[1] sc[*] v[1]; P{TRiP.HMS01666}attP2/TM3, Sb[1]	Bloomington Drosophila Stock Center	#38519
mtd mutant y[1] w[*]; Mi{y[+mDint2]=MIC}mtd[MI02920]/TM3, Sb[1] Ser[1]	Bloomington Drosophila Stock Center	#76158
hOXR1 overexpression w1118; P{UAS-OXR1.HA}1	Bloomington Drosophila Stock Center	#64104
hOXR1 overexpression w1118; P{UAS-OXR1.HA}4/TM3, Sb1	Bloomington Drosophila Stock Center	#64105
Fdxh RNAi w1118; P{GD1274}v24497	Vienna Drosophila Resource Center	#24497
CG15515 RNAi w1118; P{GD8577}v39872	Vienna Drosophila Resource Center	#39872
tj RNAi y[1] sc[*] v[1]; P{TRiP.HMS01069}attP2	Bloomington Drosophila Stock Center	#34595
TJ-GFP w[1118]; P33657Bac{y[+mDint2] w[+mC]=tj-GFP.FPTB}VK00033	Bloomington Drosophila Stock Center	#66391
ctcf RNAi y[1] sc[*] v[1]; P{TRiP.GL00266}attP2	Bloomington Drosophila Stock Center	#35354
ctcf RNAi y[1] v[1]; P{TRiP.HMS02017}attP40	Bloomington Drosophila Stock Center	#40850
vps26 RNAi y[1] v[1]; P{TRiP.HMS01769}attP40	Bloomington Drosophila Stock Center	#38937
vps29 RNAi y[1] v[1]; P{TRiP.HMJ21316}attP40	Bloomington Drosophila Stock Center	#53951
vps35 RNAi	Bloomington Drosophila Stock Center	#38944

y[1] sc[*] v[1] sev2[1]; P{TRiP.HMS01858}attP40		
Atg8 overexpression y[1] w[1118]; P{w[+mC]=UASp-GFP-mCherry-Atg8a}2	Bloomington Drosophila Stock Center	#37749
hLAMP1 overexpression y[1] w[*]; PBac{y[+mDint2] w[+mC]=UAS-hLAMP1.HA}VK00033	Bloomington Drosophila Stock Center	#86301
Atg1 overexpression y[1] w[*]; P{w[+mC]=UAS-Atg1.S}6A	Bloomington Drosophila Stock Center	#51654

Cell lines used		
Line	Source	ID
F0062.1 Human skin fibroblasts Healthy	Provided by laboratory of Dr. Philippe Campeau, CHU Sainte Justine Research Center, Montreal, QC, Canada	N/A
F0342.1 Male human skin fibroblasts OXR1 mutation c.1324delA p.Ser44Valfs*2	Provided by laboratory of Dr. Philippe Campeau, CHU Sainte Justine Research Center, Montreal, QC, Canada	N/A
Schneider's 2 *Drosophila* embryonic cell line	Drosophila Genomic Resource Center	#6

Cell and fly media and additives used		
Schneider's insect medium	Quartzy	Cat#S0146
Dulbecco's modification of Eagle's medium, Corning	VWR	Cat#45000-304
Fetal bovine serum	Life Technologies	Cat#10082147
Penicillin-streptomycin	Life Technologies	Cat#15140122
Nutri-Fly Drosophila Agar, Gelidium	Genesee Scientific	Cat#66-104
Yellow Cornmeal	Genesee Scientific	Cat#62-100
Pure Cane Granulated Sugar	C&H	N/A
Bacto yeast extract	VWR	Cat#90000-722
Saf instant yeast	Rainy Day Foods	

Primers used		
mtd Forward	Integrated DNA Technologies	GAAGAAGACTCCAAGGAGCT
mtd Reverse	Integrated DNA Technologies	CCCTATTTCTGCATCTAAGCG
Bgl2 mtd promoter Fr Forward	Integrated DNA Technologies	GGAAGATCTGTGTACATATTGAATCAAATCAGC
Xho1 mtd promoter Fr Reverse	Integrated DNA Technologies	TACGCTCGAGTTCTAGCCCTGTATCATACGG
s-188-cc Forward	Integrated DNA Technologies	GACGGCCAGTGCCAAGCTATCGATAGG
s-188-cc Reverse	Integrated DNA Technologies	GCGCTACAGGTTTCTTGGGGCCCAAG
tj Forward	Integrated DNA Technologies	GATTCTGGTGAACACATCTTCGG
tj Reverse	Integrated DNA Technologies	TGGTGTGCGTAAGTCTGAGC
ctcf Forward	Integrated DNA Technologies	GAGCGCCAACTCCAAGATCA
ctcf Reverse	Integrated DNA Technologies	CCCATCGCCATACTCCTCAT
mtd gene region Forward (for TJ ChIP)	Integrated DNA Technologies	GACCTCGAAAGAGTCGCCAT
mtd gene region Forward (for TJ ChIP)	Integrated DNA Technologies	GATTCAGGGAATTGTGCGCC
mtd-RM Forward	Integrated DNA Technologies	TGGAAGACCTCGAAAGAGT
mtd-RM Reverse	Integrated DNA Technologies	CGAGTTCTCGGTTATCTACC
mtd long transcripts Forward	Integrated DNA Technologies	TCGACTTGGACTCGCTCCG
mtd long transcripts Reverse	Integrated DNA Technologies	TGGGTATGGTGGGCAATGAAG
mtd-RF, RAA transcripts Forward	Integrated DNA Technologies	GAGAGCCGGATAATCCACGA
mtd-RF, RAA transcripts Reverse	Integrated DNA Technologies	TCTCCATTGCGCCAGAAGAC
mtd-RA, RB, RI transcripts Forward	Integrated DNA Technologies	AAAAACTTACGGCCACGCTG
mtd-RA, RB, RI transcripts Reverse	Integrated DNA Technologies	TATTTCCCAGCGTCTCGTCG
mtd-RQ, RH transcripts Forward	Integrated DNA Technologies	GCTGAATATGTTCGCCGCC

mtd-RQ, RH transcripts Reverse	Integrated DNA Technologies	AAGCACTTGCAGAACATATAGAAAT
mtd-RC transcript Forward	Integrated DNA Technologies	GAAGAGCGGAAGGCGTAGAG
mtd-RC transcript Reverse	Integrated DNA Technologies	AAACGGCCAAGATGCCAAAC
hOXR1 Forward	Integrated DNA Technologies	GGTTTGCTGTGCCACAAG
hOXR1 Reverse	Integrated DNA Technologies	GGTTCTCTGGTATATTCGCCAG
RpL32 Forward	Integrated DNA Technologies	TAAGCTGTCGCACAAATGG
RpL32 Reverse	Integrated DNA Technologies	GGCATCAGATACTGTCCCT
Act5C Forward	Integrated DNA Technologies	AAGTACCCCATTGAGCACGG
Act5C Reverse	Integrated DNA Technologies	ACATACATGGCGGGTGTGTT

Antibodies and Stains		
Rabbit polyclonal anti-OXR1	Invitrogen	Cat#PA5-72405
Rabbit polyclonal anti-OXR1	abcam	Cat#ab103042
Goat polyclonal anti-VPS35	abcam	Cat#ab10099
Rabbit polyclonal anti-VPS26A	Proteintech	Cat#12804-1-AP
Rabbit polyclonal anti-LC3B	Novus Biologicals	Cat#NB100-2220
Rabbit polyclonal anti-Atg8	Sigma-Aldrich	Cat#ABC974
Mouse monoclonal anti-Cathepsin B	abcam	Cat#ab58802
Rabbit monoclonal anti-GAPDH	abcam	Cat#ab9485
Rabbit polyclonal anti-β-actin	Cell Signaling	Cat#4967
Mouse monocolonal anti-α-Tubulin	Sigma-Aldrich	Cat#T6199
Mouse monoclonal anti-Rab7	abcam	Cat#ab50533
Mouse monoclonal anti-elav	DSHB	Cat#Elav-9F8A9
Mouse monoclonal anti-ATP5A	abcam	Cat#ab14748
Mouse monoclonal anti-LAMP1	abcam	Cat#ab25630
Mouse monoclonal anti-Calreticulin	abcam	Cat#ab22683
Mouse polyclonal anti-GM130	abcam	Cat#ab169276
Mouse monoclonal anti-GFP	Santa Cruz Biotech	Cat#sc-9996
Sheep anti-Mouse IgG HRP-linked secondary	Sigma Aldrich	Cat#NXA931V
Donkey anti-Rabbit IgG HRP-linked secondary	Sigma Aldrich	Cat#NA934V
Mouse anti-Goat IgG HRP-conjugated secondary	Santa Cruz Biotech	Cat#sc-2354
Alexa Fluor 488 donkey anti-rabbit IgG (H+L) secondary	Invitrogen	Cat#A21206
Alexa Fluor 647 donkey anti-goat IgG (H+L) secondary	Invitrogen	Cat#A21447
Alexa Fluor 647 donkey anti-mouse IgG (H+L) secondary	Invitrogen	Cat#A21238
LysoTracker™ Deep Red	Thermo Fisher	Cat#L12492
Hoescht 33342 Solution	Thermo Fisher	Cat#62249

Data and materials availability

Any additional information required to reanalyze the data reported in this paper is available from the lead contact upon request. RNA-seq data is available via the Gene Expression Omnibus (GEO) repository. Raw data and complete MS data sets have been uploaded to the Center for Computational Mass Spectrometry, to the MassIVE repository at UCSD, and can be downloaded using the following link: https://massive.ucsd.edu/ProteoSAFe/dataset.jsp?task=d8f8a278868d42398c9ba8c772395c7b (MassIVE ID number: MSV000088897; ProteomeXchange ID: PXD031837).

references

1 Mattson, M. P. Gene-diet interactions in brain aging and neurodegenerative disorders. *Ann Intern Med* **139**, 441-444 (2003).

2 Wilson, K. A. *et al.* Evaluating the beneficial effects of dietary restrictions: A framework for precision nutrigeroscience. *Cell metabolism* **33**, 2142-2173, doi:10.1016/j.cmet.2021.08.018 (2021).

3 Mackay, T. F. *et al.* The Drosophila melanogaster Genetic Reference Panel. *Nature* **482**, 173-178, doi:10.1038/nature10811 (2012).

4 Wilson, K. A. *et al.* GWAS for Lifespan and Decline in Climbing Ability in Flies upon Dietary Restriction Reveal decima as a Mediator of Insulin-like Peptide Production. *Curr Biol* **30**, 2749-2760 e2743, doi:10.1016/j.cub.2020.05.020 (2020).

5 Wang, J. *et al.* Loss of Oxidation Resistance 1, OXR1, Is Associated with an Autosomal-Recessive Neurological Disease with Cerebellar Atrophy and Lysosomal Dysfunction. *Am J Hum Genet* **105**, 1237-1253, doi:10.1016/j.ajhg.2019.11.002 (2019).

6 Liu, K. X. *et al.* Neuron-specific antioxidant OXR1 extends survival of a mouse model of amyotrophic lateral sclerosis. *Brain* **138**, 1167-1181, doi:10.1093/brain/awv039 (2015).

7 Small, S. A. & Petsko, G. A. Retromer in Alzheimer disease, Parkinson disease and other neurological disorders. *Nat Rev Neurosci* **16**, 126-132, doi:10.1038/nrn3896 (2015).

8 Gallon, M. & Cullen, P. J. Retromer and sorting nexins in endosomal sorting. *Biochem Soc Trans* **43**, 33-47, doi:10.1042/BST20140290 (2015).

9 Volkert, M. R., Elliott, N. A. & Housman, D. E. Functional genomics reveals a family of eukaryotic oxidation protection genes. *Proceedings of the National Academy of Sciences of the United States of America* **97**, 14530-14535, doi:10.1073/pnas.260495897 (2000).

10 Xu, H. *et al.* Zebrafish Oxr1a Knockout Reveals Its Role in Regulating Antioxidant Defenses and Aging. *Genes (Basel)* **11**, doi:10.3390/genes11101118 (2020).

11 Finelli, M. J., Sanchez-Pulido, L., Liu, K. X., Davies, K. E. & Oliver, P. L. The Evolutionarily Conserved Tre2/Bub2/Cdc16 (TBC), Lysin Motif (LysM), Domain Catalytic (TLDc) Domain Is Neuroprotective against Oxidative Stress. *The Journal of biological chemistry* **291**, 2751-2763, doi:10.1074/jbc.M115.685222 (2016).

12 Slattery, M. *et al.* Diverse patterns of genomic targeting by transcriptional regulators in Drosophila melanogaster. *Genome Res* **24**, 1224-1235, doi:10.1101/gr.168807.113 (2014).

13 Negre, N. *et al.* A cis-regulatory map of the Drosophila genome. *Nature* **471**, 527-531, doi:10.1038/nature09990 (2011).

14 Lachmann, A. *et al.* Massive mining of publicly available RNA-seq data from human and mouse. *Nature communications* **9**, 1366, doi:10.1038/s41467-018-03751-6 (2018).

15 Maruzs, T. *et al.* Retromer Ensures the Degradation of Autophagic Cargo by Maintaining Lysosome Function in Drosophila. *Traffic* **16**, 1088-1107, doi:10.1111/tra.12309 (2015).

16 Cui, Y. *et al.* Retromer has a selective function in cargo sorting via endosome transport carriers. *The Journal of cell biology* **218**, 615-631, doi:10.1083/jcb.201806153 (2019).

17 Lane, R. F. *et al.* Vps10 family proteins and the retromer complex in aging-related neurodegeneration and diabetes. *J Neurosci* **32**, 14080-14086, doi:10.1523/JNEUROSCI.3359-12.2012 (2012).

18 Wilson, K. A. The understudied links of the retromer complex to age-related pathways. *Geroscience* **44**, 19-24, doi:10.1007/s11357-021-00430-1 (2022).

19 Lin, G. *et al.* Phospholipase PLA2G6, a Parkinsonism-Associated Gene, Affects Vps26 and Vps35, Retromer Function, and Ceramide Levels, Similar to alpha-Synuclein Gain. *Cell metabolism* **28**, 605-618 e606, doi:10.1016/j.cmet.2018.05.019 (2018).

20 Vagnozzi, A. N. & Pratico, D. Endosomal sorting and trafficking, the retromer complex and neurodegeneration. *Molecular psychiatry* **24**, 857-868, doi:10.1038/s41380-018-0221-3 (2019).

21 Mecozzi, V. J. *et al.* Pharmacological chaperones stabilize retromer to limit APP processing. *Nat Chem Biol* **10**, 443-449, doi:10.1038/nchembio.1508 (2014).

22 Yoshii, S. R. & Mizushima, N. Monitoring and Measuring Autophagy. *International journal of molecular sciences* **18**, doi:10.3390/ijms18091865 (2017).

23 Wang, S. *et al.* The retromer complex is required for rhodopsin recycling and its loss leads to photoreceptor degeneration. *PLoS biology* **12**, e1001847, doi:10.1371/journal.pbio.1001847 (2014).

24 Kusne, Y., Wolf, A. B., Townley, K., Conway, M. & Peyman, G. A. Visual system manifestations of Alzheimer's disease. *Acta Ophthalmol* **95**, e668-e676, doi:10.1111/aos.13319 (2017).

25 Roberts, R. O. *et al.* Association Between Olfactory Dysfunction and Amnestic Mild Cognitive Impairment and Alzheimer Disease Dementia. *JAMA Neurol* **73**, 93-101, doi:10.1001/jamaneurol.2015.2952 (2016).

26 Bruderer, R. *et al.* Optimization of Experimental Parameters in Data-Independent Mass Spectrometry Significantly Increases Depth and Reproducibility of Results. *Molecular & cellular*

proteomics : MCP **16**, 2296-2309, doi:10.1074/mcp.RA117.000314 (2017).

27 Johnson, E. C. B. *et al.* Large-scale deep multi-layer analysis of Alzheimer's disease brain reveals strong proteomic disease-related changes not observed at the RNA level. *Nat Neurosci*, doi:10.1038/s41593-021-00999-y (2022).

28 Jia, K., Cui, C., Gao, Y., Zhou, Y. & Cui, Q. An analysis of aging-related genes derived from the Genotype-Tissue Expression project (GTEx). *Cell Death Discov* **4**, 26, doi:10.1038/s41420-018-0093-y (2018).

29 Mele, M. *et al.* Human genomics. The human transcriptome across tissues and individuals. *Science* **348**, 660-665, doi:10.1126/science.aaa0355 (2015).

30 Chen, E. Y. *et al.* Enrichr: interactive and collaborative HTML5 gene list enrichment analysis tool. *BMC Bioinformatics* **14**, 128, doi:10.1186/1471-2105-14-128 (2013).

31 Simoes, S. *et al.* Tau and other proteins found in Alzheimer's disease spinal fluid are linked to retromer-mediated endosomal traffic in mice and humans. *Science translational medicine* **12**, doi:10.1126/scitranslmed.aba6334 (2020).

32 Qureshi, Y. H. *et al.* The neuronal retromer can regulate both neuronal and microglial phenotypes of Alzheimer's disease. *Cell reports* **38**, 110262, doi:10.1016/j.celrep.2021.110262 (2022).

33 Simoes, S. *et al.* Alzheimer's vulnerable brain region relies on a distinct retromer core dedicated to endosomal recycling. *Cell reports* **37**, 110182, doi:10.1016/j.celrep.2021.110182 (2021).

34 Moulton, M. J. *et al.* Neuronal ROS-induced glial lipid droplet formation is altered by loss of Alzheimer's disease-associated genes. *Proceedings of the National Academy of Sciences of the United States of America* **118**, doi:10.1073/pnas.2112095118 (2021).

35 Johnson, E. C. B. *et al.* Large-scale proteomic analysis of Alzheimer's disease brain and cerebrospinal fluid reveals early changes in energy metabolism associated with microglia and astrocyte activation. *Nature medicine* **26**, 769-780, doi:10.1038/s41591-020-0815-6 (2020).

36 Katewa, S. D. *et al.* Intramyocellular fatty-acid metabolism plays a critical role in mediating responses to dietary restriction in Drosophila melanogaster. *Cell metabolism* **16**, 97-103, doi:10.1016/j.cmet.2012.06.005 (2012).

37 Wilson, K. A. *et al.* Evaluating the beneficial effects of dietary restrictions: A framework for precision nutrigeroscience. *Cell metabolism*, doi:10.1016/j.cmet.2021.08.018 (2021).

38 Knupp, A. *et al.* Depletion of the AD Risk Gene SORL1 Selectively Impairs Neuronal Endosomal Traffic Independent of Amyloidogenic APP Processing. *Cell reports* **31**, 107719, doi:10.1016/j.celrep.2020.107719 (2020).

39 Pandey, S., Dhusia, K., Katara, P., Singh, S. & Gautam, B. An in silico analysis of deleterious single nucleotide polymorphisms and molecular dynamics simulation of disease linked mutations in genes responsible for neurodegenerative disorder. *J Biomol Struct Dyn*, 1-14, doi:10.1080/07391102.2019.1682047 (2019).

40 Li, J. G., Chiu, J., Ramanjulu, M., Blass, B. E. & Pratico, D. A pharmacological chaperone improves memory by reducing Abeta and tau neuropathology in a mouse model with plaques and tangles. *Molecular neurodegeneration* **15**, 1, doi:10.1186/s13024-019-0350-4 (2020).

41 Li, J. G., Chiu, J. & Pratico, D. Full recovery of the Alzheimer's disease phenotype by gain of function of vacuolar protein sorting 35. *Mol Psychiatry*, doi:10.1038/s41380-019-0364-x (2019).

42 Muhammad, A. *et al.* Retromer deficiency observed in Alzheimer's disease causes hippocampal dysfunction, neurodegeneration, and Abeta accumulation. *Proceedings of the National Academy of Sciences of the United States of America* **105**, 7327-7332, doi:10.1073/pnas.0802545105 (2008).

43 Mir, R. *et al.* The Parkinson's disease VPS35[D620N] mutation enhances LRRK2-mediated Rab protein phosphorylation in mouse and human. *The Biochemical journal* **475**, 1861-1883, doi:10.1042/BCJ20180248 (2018).

44 Chen, X. *et al.* Parkinson's disease-linked D620N VPS35 knockin mice manifest tau neuropathology and dopaminergic neurodegeneration. *Proceedings of the National Academy of Sciences of the United States of America* **116**, 5765-5774, doi:10.1073/pnas.1814909116 (2019).

45 Zhao, Y. *et al.* Reduced LRRK2 in association with retromer dysfunction in post-mortem brain tissue from LRRK2 mutation carriers. *Brain* **141**, 486-495, doi:10.1093/brain/awx344 (2018).

46 Danson, C. M., Pearson, N., Heesom, K. J. & Cullen, P. J. Sorting nexin-21 is a scaffold for the endosomal recruitment of huntingtin. *J Cell Sci* **131**, doi:10.1242/jcs.211672 (2018).

47 Finan, G. M., Okada, H. & Kim, T. W. BACE1 retrograde trafficking is uniquely regulated by the cytoplasmic domain of sortilin. *The Journal of biological chemistry* **286**, 12602-12616, doi:10.1074/jbc.M110.170217 (2011).

48 Nelson, C. S. *et al.* Cross-phenotype association tests uncover genes mediating nutrient response in Drosophila. *BMC Genomics* **17**, 867, doi:10.1186/s12864-016-3137-9 (2016).

49 Virtanen, P. *et al.* SciPy 1.0: fundamental algorithms for scientific computing in Python. *Nature methods* **17**, 261-272, doi:10.1038/s41592-019-0686-2 (2020).

50 David, L. A. *et al.* Diet rapidly and reproducibly alters the human gut microbiome. *Nature* **505**, 559-563, doi:10.1038/nature12820 (2014).

51 Kulahoglu, C. & Brautigam, A. Quantitative transcriptome analysis using RNA-seq. *Methods in molecular biology* **1158**, 71-91, doi:10.1007/978-1-4939-0700-7_5 (2014).

52 Cook, K. R., Parks, A. L., Jacobus, L. M., Kaufman, T. C. & Matthews, K. A. New research resources at the Bloomington Drosophila Stock Center. *Fly (Austin)* **4**, 88-91 (2010).

53 Vissers, J. H., Manning, S. A., Kulkarni, A. & Harvey, K. F. A Drosophila RNAi library modulates Hippo pathway-dependent tissue growth. *Nature communications* **7**, 10368, doi:10.1038/ncomms10368 (2016).

54 Bischof, J., Sheils, E. M., Bjorklund, M. & Basler, K. Generation of a transgenic ORFeome library in Drosophila. *Nature protocols* **9**, 1607-1620, doi:10.1038/nprot.2014.105 (2014).

55 Zid, B. M. *et al.* 4E-BP extends lifespan upon dietary restriction by enhancing mitochondrial activity in Drosophila. *Cell* **139**, 149-160, doi:10.1016/j.cell.2009.07.034 (2009).

56 Katewa, S. D. *et al.* Peripheral Circadian Clocks Mediate Dietary Restriction-Dependent Changes in Lifespan and Fat Metabolism in Drosophila. *Cell Metab* **23**, 143-154, doi:10.1016/j.cmet.2015.10.014 (2016).

57 Osterwalder, T., Yoon, K. S., White, B. H. & Keshishian, H. A conditional tissue-specific transgene expression system using inducible GAL4. *Proceedings of the National Academy of Sciences of the United States of America* **98**, 12596-12601, doi:10.1073/pnas.221303298 (2001).

58 Arya, G. H. *et al.* The genetic basis for variation in olfactory behavior in Drosophila melanogaster. *Chemical senses* **40**, 233-243, doi:10.1093/chemse/bjv001 (2015).

59 Iyer, J. *et al.* Quantitative Assessment of Eye Phenotypes for Functional Genetic Studies Using Drosophila melanogaster. *G3* **6**, 1427-1437, doi:10.1534/g3.116.027060 (2016).

60 Hu, X., Cherbas, L. & Cherbas, P. Transcription activation by the ecdysone receptor (EcR/USP): identification of activation functions. *Mol Endocrinol* **17**, 716-731 (2003).

61 Escher, C. *et al.* Using iRT, a normalized retention time for more targeted measurement of peptides. *Proteomics* **12**, 1111-1121, doi:10.1002/pmic.201100463 (2012).

62 Gillet, L. C. *et al.* Targeted data extraction of the MS/MS spectra generated by data-independent acquisition: a new concept for consistent and accurate proteome analysis. *Molecular & cellular proteomics : MCP* **11**, O111 016717, doi:10.1074/mcp.O111.016717 (2012).

63 Collins, B. C. *et al.* Multi-laboratory assessment of reproducibility, qualitative and quantitative performance of SWATH-mass spectrometry. *Nature communications* **8**, 291, doi:10.1038/s41467-017-00249-5 (2017).

64 Burger, T. Gentle Introduction to the Statistical Foundations of False Discovery Rate in Quantitative Proteomics. *Journal of proteome research***17**, 12-22, doi:10.1021/acs.jproteome.7b00170 (2018).

Declarations

Acknowledgements

We would like to thank the members of the Kapahi and Ellerby labs as well as Dr. Malene Hansen and Dr. Gary Howard for their comments throughout the manuscript and experiments. KAW is supported by NIH grant T32AG000266-23. SB is supported by Larry L. Hillblom Foundation fellowship 2019-A-026-FEL. TAUH was supported by NIH grant 5F31AG062112. HJB is supported by NIH grants R01AG07326 and U01AG072439. Support of instrumentation for the Orbitrap Eclipse Tribrid from the NCRR shared instrumentation grant 1S10 OD028654, awarded to BS. LME is supported by NIH grant R01AG061879. PK is supported by NIH grant R01AG061165 and the Larry L. Hillblom Foundation. LME and PK are supported by NIH grant R56AG070705-01. We thank the UC Berkeley qb3 Functional Genomics Laboratory for the RNA sequencing referenced in Figures 3a, 3b, and Extended Data Figure 2b. Figures 2a, 4b, and Extended Data Figure 1g were generated with the use of BioRender.com.

Author contributions

Conceptualization: KAW, LME, PK

Methodology: KAW, SB, EBD, GC, RBB, HJB, BS, NTS, LME, PK

Investigation: KAW, SB, EBD, BAH, EMC, TAUH, JB, GWB, JNB, JR, MGP, CSN, AA, GC

Visualization: KAW, SB, GC

Funding acquisition: KAW, TAUH, HJB, BS, LME, PK

Project administration: PMC, LME, PK

Supervision: LME, PK

Writing – original draft: KAW, LME, PK

Writing – review & editing: KAW, SB, EBD, BAH, EMC, TAUH, JB, GWB, JNB, JR, MGP, CSN, AA, GC, RBB, PMC, HJB, BS, NTS, LME, PK

Competing interests

PK is founder and a member of the scientific advisory board at Juvify Bio. The other authors have no conflicts of interest.

Additional information

Supplementary Information is available for this paper.

Correspondence and requests for materials should be addressed to Pankaj Kapahi (pkapahi@buckinstitute.org).

Figures

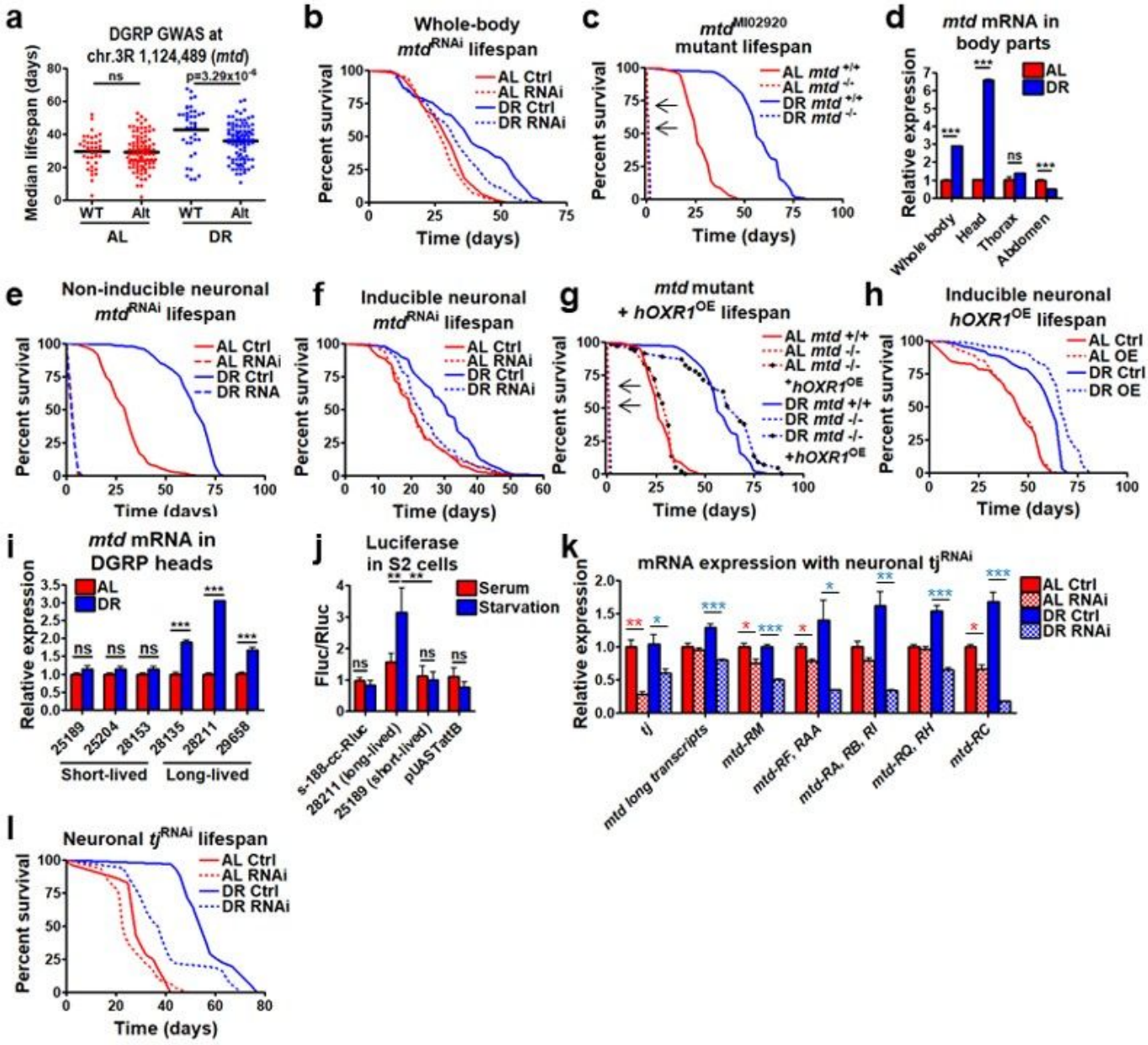

Figure 1

***mtd* is upregulated allele-specifically by Traffic Jam (TJ) to extend lifespan under DR.**

a, DGRP strains aligned by wildtype or alternative (Alt) allele in *mtd* gene region. Dots represent median strain lifespan on AL (red) or DR (blue). Black bars represent mean across all strains. **b**, Survival of whole-body mtd^{RNAi} (dashed) and controls (solid). **c**, Survival of $mtd^{MI02920}$ mutant. **d**, *mtd* mRNA in w^{1118} fly body parts, normalized to AL. **e**, Survival of constitutively active pan-neuronal mtd^{RNAi}. **f**, Survival of inducible pan-neuronal mtd^{RNAi}. **g**, Survival curve of $mtd^{MI02920}$ flies (dashed), controls (solid), and $mtd^{MI02920}$ mutants with *mtd-Gal4*-driven $hOXR1^{OE}$ (dashed with circles). **h**, Survival of inducible pan-neuronal $hOXR1^{OE}$. **i**, *mtd* mRNA in heads of DGRP strains with either the short-lived (left) or long-lived (right) allele after 7 days on AL or DR. **j**, Luciferase activity in S2 cells transfected with cloned variant alleles from DGRP strains. **k**, mRNA of *tj*, *mtd* long transcripts, or specific shorter *mtd* transcripts in fly heads with constitutively active pan-neuronal tj^{RNAi}, normalized to AL. **l**, Survival of inducible pan-neuronal tj^{RNAi} and controls.

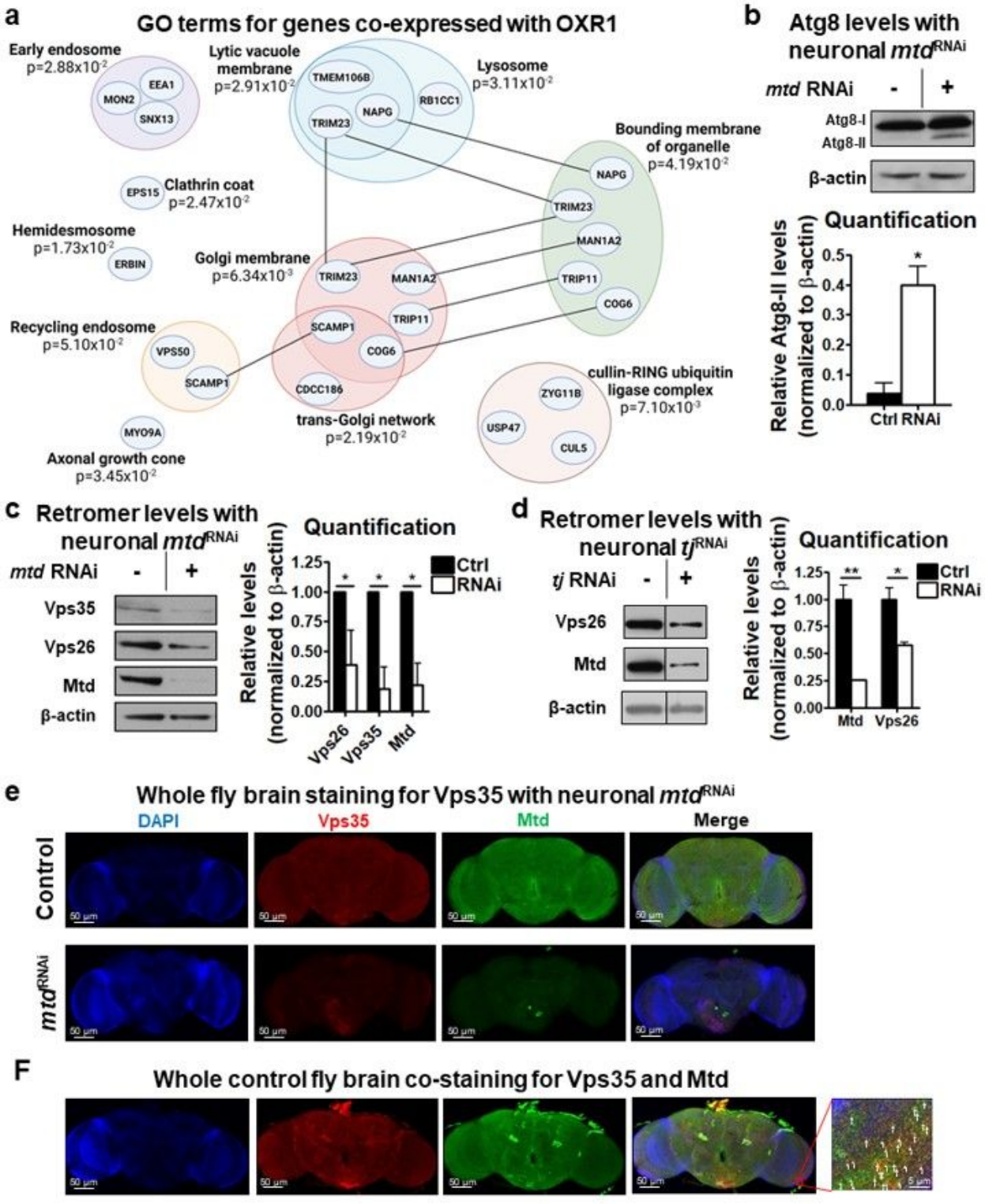

Figure 2

mtd is required for retromer maintenance.

a, GO term enrichment for top 50 genes co-expressed with OXR1, arranged by organelle and function. **b**, Western blot for Atg8 in fly heads with constitutively active pan-neuronal *mtd*^{RNAi}. **c**, Vps35 and Vps26 levels in heads with constitutively active pan-neuronal *mtd*^{RNAi}. **d**, Vps26 and Mtd levels in heads with

constitutively active pan-neuronal *tj*^{RNAi}. **e**, Immunohistochemistry of brains from flies under control conditions (top) or pan-neuronal *mtd*^{RNAi} (bottom), probed for DAPI (blue), Vps35 (red), and Mtd (green). **f**, Immunohistochemistry of *w*^{1118} fly brains probed for DAPI (blue), Vps35 (red), and Mtd (green). Image on right is magnified from boxed region in whole-brain images.

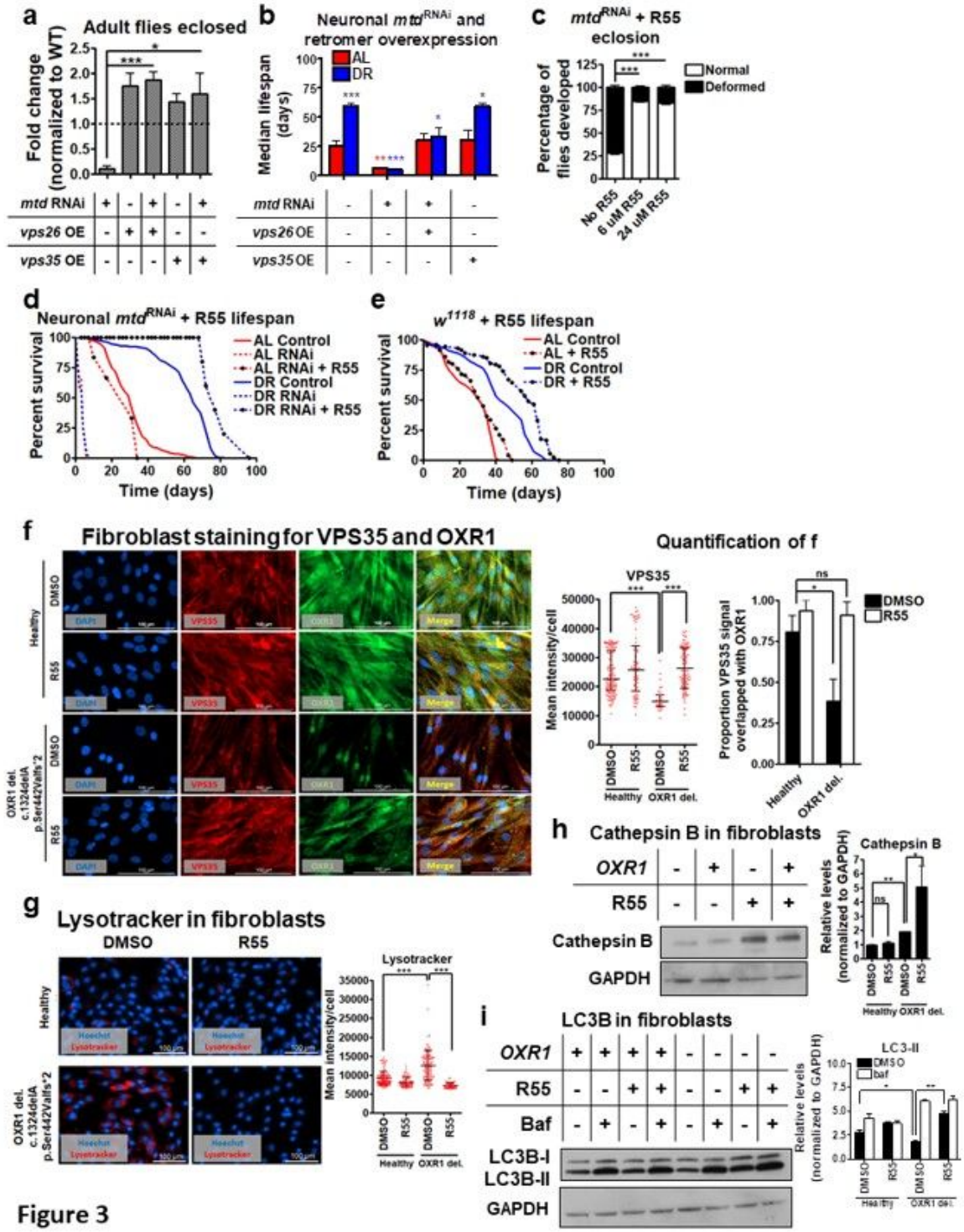

Figure 3

Retromer stabilization rescues neuronal *mtd/OXR1* deficiency in flies and human fibroblasts.

a, Number of flies eclosing in control conditions, with neuronal mtd^{RNAi}, with $vps26^{OE}$ or $vps35^{OE}$, or with simultaneous mtd^{RNAi} and $vpsS26^{OE}$ or $vpsS35^{OE}$, normalized to controls. **b**, Median lifespan of control flies, constitutively active pan-neuronal mtd^{RNAi}, or simultaneous mtd^{RNAi} and $vps26^{OE}$ or $vps35^{OE}$. **c**, Percentage of healthy flies developed with constitutively active pan-neuronal mtd^{RNAi} or supplementation with 6 μM or 24 μM R55. **d**, Survival of constitutively active pan-neuronal mtd^{RNAi} (dashed), background controls (solid), and mtd^{RNAi} supplemented with 6 μM R55 (dashed with circles). **e**, Survival of w^{1118} flies reared with or without 6 μM R55. **f**, Immunocytochemistry of healthy patient fibroblasts or patients with OXR1 mutation (c.132delA) with or without 10 μM R55 treatment. DAPI in blue, OXR1 in green, VPS35 in red. **g**, Live cell imaging of fibroblasts with normal *OXR1* or homozygous mutation. Nucleus stained with Hoechst (blue), lysosomes stained with LysoTracker (red). LysoTracker intensity per cell quantified beside images. **h**, Cathepsin B levels in normal *OXR1* or mutant fibroblasts treated with or without 10 μM R55. **i**, LC3-II levels normalized to GAPDH with or without bafilomycin (baf) treatment, with DMSO or 10 μM R55.

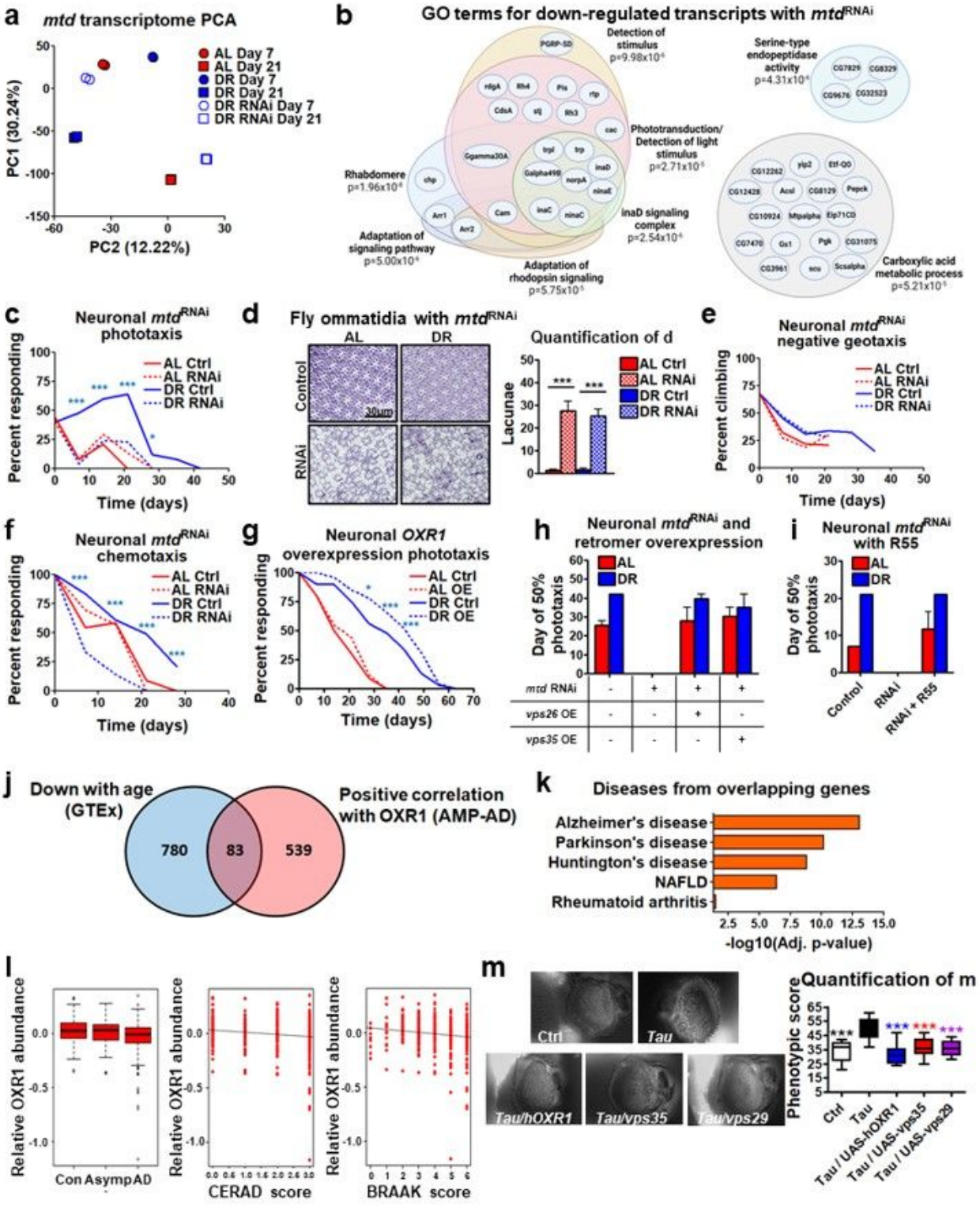

Figure 4

Retromer stabilization by R55 or OXR1 overexpression preserves vision and rescues tauopathy.

a, PCA of fly head transcriptomes with and without inducible pan-neuronal *mtd*^{RNAi} at day 7 or 21. **b**, GO terms from RNA sequencing analysis, comparing transcripts downregulated in heads from inducible pan-neuronal *mtd*^{RNAi} flies undergoing DR. **c**, Phototaxis in flies with inducible pan-neuronal *mtd*^{RNAi}. **d**, Fly

ommatidia with or without constitutively active pan-neuronal *mtd*^{RNAi}. Image quantification on right. **e**, Negative geotaxis in flies with inducible pan-neuronal *mtd*^{RNAi}. **f**, Chemotaxis in flies with inducible pan-neuronal *mtd*^{RNAi}. **g**, Phototaxis in flies with inducible pan-neuronal *hOXR1*^{OE}. **h**, Day of 50% decline in phototaxis response in control flies, constitutively active pan-neuronal *mtd*^{RNAi}, or simultaneous *mtd*^{RNAi} and *vps26*^{OE} or *vps35*^{OE}. Flies with *mtd*^{RNAi} alone had no response. **i**, Day of 50% decline in phototaxis response in control flies, constitutively active pan-neuronal *mtd*^{RNAi}, or simultaneous *mtd*^{RNAi} and 6 μM R55 treatment. Untreated flies with *mtd*^{RNAi} alone had no response. **j**, Venn diagram of genes downregulated in GTEx dataset and proteins positively correlated with OXR1 from AMP-AD dataset. **k**, Diseases enriched from overlapping genes in **j**. **l**, Correlation of OXR1 protein abundance with AD diagnosis (left), CERAD score (middle), and BRAAK score (right). Asymp = asymptomatic AD. **m**, Eye images and quantification of degenerative phenotype in control fly eyes, constitively active mutant *Tau*^{OE} driven by *GMR*, or *GMR-Tau*^{OE} with simultaneous neuronal *hOXR1*^{OE}, *Vps35*^{OE}, or *Vps29*^{OE}.

Supplementary Files

This is a list of supplementary files associated with this preprint. Click to download.

- SupplementaryData.xlsx
- ExtendedDataFigures.docx